

Contents lists available at ScienceDirect

# Water Resources and Industry

journal homepage: www.elsevier.com/locate/wri



# Removal of Acid Blue 80 from aqueous solutions using chitosan-based beads modified with choline chloride:urea Deep Eutectic Solvent and FeO

Lucía Blanco, Oscar Martínez-Rico, Ángeles Domínguez, Begoña González

Chemical Engineering Department, Universidade de Vigo, Spain

### ARTICLE INFO

Keywords:
Chitosan-deep eutectic solvent beads
Anthraquinone dye
Acid blue 80
Textile pollution mitigation
Adsorption

### ABSTRACT

An alternative chitosan-based adsorbent modified by impregnation with deep eutectic solvent (DES) choline-chloride:urea at a molar ratio 1:2 proved efficient removal of the anthraquinone dye Acid Blue 80 (AB80) from aqueous solutions, and offered enhanced adsorption capacity compared to the starting materials. The adsorption was mainly affected by initial AB80 concentration, adsorbent dosage, contact time, and slightly influenced by temperature (25–45 °C), and pH (3.5–10). The pseudo-second-order kinetic model fitted the experimental data, and pseudo-first order model fitted as well at the highest AB80 concentration, 250 mg/L. The experimental data agreed with the Langmuir isotherm model, with a maximum adsorption capacity of 61.64 mg/g at 35 °C. The process was exothermic above 100 mg/L of dye and spontaneous up to 200 mg/L (T < 35 °C). The adsorbent could be reused without further treatment at least 5 times providing  $\geq$ 40% removal, whereas the dye could be efficiently recovered by NaOH desorption. Electrostatic interactions as well as physisorption could explain the adsorption behavior.

# Credit author statement

Lucia Blanco: investigation, writing-original draft. Oscar Martínez-Rico: investigation, validation.

Ángeles Domínguez: supervision, funding acquisition, conceptualization.

Begoña González: supervision, funding acquisition, Project administration.

### 1. Introduction

Water resources are of utmost importance, in a world facing challenges such as the population growth, the climate change and the

Abbreviations: un-Ch, unmodified chitosan beads; Ch-DES, DES-modified chitosan beads; Ch-FeO-DES, DES modified chitosan-FeO beads; AB80, Acid Blue 80; HBD, hydrogen bond donor; HBA, hydrogen bond acceptor; DES, deep eutectic solvent; ILs, ionic liquids; FTIR, Fourier transform infrared spectrum; ATR, Attenuated Total Reflection Spectroscopy; SEM, Scanning electron microscopy; BET, Brunauer-Emmett-Teller surface area analysis; BJH, Barrett-Joyner-Halenda pore size and volume analysis; ChCl, choline chloride.

E-mail address: bgp@uvigo.es (B. González).

<sup>\*</sup> Corresponding author.

increasing need for water in agriculture and industry. However, the disposal of contaminants and the scarce effectiveness of water treatment to eliminate a number of harmful substances can result in reduced water quality, and damage to aquatic environment, but also to humans. The removal of highly toxic pollutants such as dyes, phenolic compounds, metals, pesticides and drugs, detected not only in wastewaters, but also in surface and even drinking water, is a challenge, since the conventional methods used in treatment plants do not allow their elimination [1].

The textile industry faces a serious environmental concern: the amount and the chemical load of water discharged. Water is used as the principal medium for removing impurities, applying dyes and finishing agents. Although dyestuffs do not represent a significant load compared to other substances used in the process, they cause the colour of the effluent, and this poses environmental concerns, since high doses may reduce light exposure to aquatic photosynthetic organisms. Besides the textile sector, the use of dyes has been incorporated to many industrial processes. Around 20% of global water pollution comes from dyeing and finishing textile products [2].

Anthraquinone and phthalocyanine dyes are widely employed as the primary or secondary compounds in commercial trichromatic dyeing formulations [3]. Nevertheless, there is significantly less research devoted to the treatment of anthraquinones compared to azo compounds [4]. Acid Blue 80 (AB80), an anionic anthraquinone dye with two sulfonate groups, has special relevance because of its widespread use: besides textile industry, it is used in paper chemicals and dyes, inks and toners, leather treatment products, polymers, cosmetics and personal care products, washing and cleaning products, biocides, among others. This substance is registered under the REACH Regulation, and the manufactured or imported volume to Europe is in the range 10–100 tonnes per annum [5]. This compound, due to its multi-ring aromatic structure, is rather stable, which can potentially lead to accumulations in the environment and cause long lasting harmful effects to aquatic life. Concentrations of 10–100 mg/L may cause acute toxicity to aquatic organisms [6]. That is why it is critical to develop methods to remove this compound from wastewaters.

There is intensive research in the topic of dye removal, which includes a wide variety of methods ranging from more conventional approaches like filtration, precipitation, coagulation or adsorption to more sophisticated ones like photooxidation, ozonation or biological treatments [7,8]. All these methods applied to textile wastewaters have their own advantages and disadvantages: chemical ones -like oxidation or ozonation-are very specific but give rise to by-products, such as sludges caused by chemical coagulation; biological ones, not adequate for most textile wastewaters, may not be effective for all dyes and require elaborate enzymatic productions; and physicochemical ones show good removal but tend to be expensive and the materials are often difficult to regenerate [7]. Adsorption stands out because of its efficient ability to cut down hazardous pollutants present in effluents [9]. With this method, compounds from a liquid or gaseous phase can be extracted by adhesion to the solid surface of the adsorbent. This adhesion can occur via electrostatic, van der Waals or chemical interactions. Among the main advantages, it requires a relatively simple operating procedure while offering a broad range of applicability for many pollutants like heavy metals or dyes [10]. That is why in the textile industry it is common practice to use, for example, commercial activated carbon as an adsorbent. However, ongoing work intends to find environmentally friendly substitutes that optimize the cost while maintaining efficiency, employing biomass substrates or agricultural and industrial byproducts [11–15]; this approach would allow improving solid waste management, one of the present issues to be addressed in preserving a healthy environment [10]. Combination of different methods is usually needed to address the treatment of textile wastewaters owing to the high variability of the effluent characteristics, and the chemical nature of the different colourants. For example, the adsorption process can be combined with membrane systems, such as nanofiltration [7]; metallic catalysts have been employed to provide an adsorption surface where the dyes can be degraded photochemically [16]. Indeed, the demand for simpler and greener adsorbents keeps rising: that is the case of chitosan, a natural adsorbent that is a cheap and eco-friendly alternative [8,17]. This abundant polymer is being widely studied as a biosupport to synthesize adsorbent materials. The large number of protonated amine (-NH<sub>3</sub>) and deprotonated hydroxyl (-O') functional groups along the linear cationic polysaccharide, provide high availability of active sites. Hence, it has an excellent adsorption ability, and also a tuneable structure, promoting physical, chemical and/or electrostatic bonds and allowing modifications that could improve the adsorption properties. A variety of additives have been used to modify chitosan and form composites or hybrid materials, and more recently, an increasing number of papers deal with combining chitosan with carbon-based materials [1]. Up to date, scarce studies describe the combination of chitosan with deep eutectic solvents (DESs) in the preparation of new materials for dye adsorption. DESs are chemicals resulting from the combination of two or more compounds in their pure states: a compound acting as hydrogen bond donor (HBD) and other compound as hydrogen bond acceptor (HBA), mixed in specific molar ratios, that lead to the formation of hydrogen bonds and van der Waals interactions between them, and resulting in a decrease in their respective melting temperature, thus obtaining a solvent in liquid state at wide temperature ranges [18]. DESs are simple to synthesize, and offer benefits such as cost-effectiveness, most of them are non-toxic and biodegradable, and could be the substitutes for ionic liquids (ILs) and organic sovents in extraction processes [19], but have been scarcely used for dyes removal [18].

Combinations of DES with polymers offer a promising alternative to obtain eco-friendly adsorbents with enhanced capacity to remove dyes and other pollutants from wastewaters [19–22]. In this study, we have developed alternative adsorbents by modifying chitosan beads through impregnation with a DES, choline chloride:urea in a molar ratio 1:2, to improve adsorption capacity of chitosan. Our objective was to modify the chitosan surface by attaching different functional groups acting as chelating sites, such as carbonyl functional groups, and provide a better performance as a dye adsorbent, as well as recovery and reutilization. We have prepared, characterized and assayed three chitosan-based adsorbents: unmodified chitosan beads (un-Ch), DES modified chitosan-FeO beads (Ch-FeO-DES), following a procedure already described [23] and DES-modified chitosan beads (Ch-DES), as new sorbent, and we have compared the removal of the colourant Acid Blue 80 obtained by the different adsorbents at the same experimental conditions. Further optimization was carried out, focused on the best adsorption efficiencies. The effects of contact time, adsorbent dose, initial dye concentration, adsorption kinetics and isotherms were investigated. The structures of the compounds used, and the colourant AB80, are shown in Fig. S1.

# 2. Materials and methods

### 2.1. Chemicals

The chemicals used in this work, together with the supplier, purity and CAS number, are listed in Table S1. Water Milli-Q quality (mQ) was used to prepare aqueous solutions. Chitosan used in this work was provided by Acros Organics, the MW was 100,000–300,000, and the deacetylation degree (DD), determined by Fourier Transform Infrared spectroscopy (FTIR), as described in the Supplementary material, was 84.8% DD.

### 2.2. Preparation of adsorbents

### 2.2.1. Unmodified chitosan beads

Unmodified chitosan beads (un-Ch), were prepared by ionic cross-linking procedure between opposite charges as described by others [23]. Chitosan was dissolved in acetic acid 2% (v/v), in the proportion 40 g/L, and it was mixed for at least 24 h at 60 °C, until a homogenous gel was formed. Beads were obtained by dropping the gel solution into a volume of NaOH (2.5 M) with a glass syringe. The beads stayed in the NaOH solution overnight, and were exhaustively washed with tap water to eliminate excess of NaOH, and rinsed with distilled water, until pH was in the range 6–7. Finally, they were dried at room temperature.

### 2.2.2. DES-modified chitosan beads

DES preparation: choline chloride:urea in molar ratio 1:2 were mixed and heated at 80  $^{\circ}$ C under constant stirring until a clear liquid was formed. The liquid was left to cool at room temperature. DES-modified chitosan beads (Ch-DES) were prepared as follows: the same procedure was followed to elaborate the chitosan beads, and soon after washing step, water was removed with filter paper, and immediately, beads were mixed with freshly prepared DES, in a proportion 1/1 (w/w) and stirred under vacuum at 60  $^{\circ}$ C, overnight, and let stay 24 h; then, they were washed and dried at room temperature.

# 2.2.3. DES modified chitosan-FeO beads

The chitosan gel was prepared as described above. A procedure of synthesis of iron oxide nanoparticles by co-precipitation was applied as described by Patiño-Ruiz et al. (2020) [23]. In brief, about 250 mL of  $FeCl_3 \cdot 6H_2O$  (0.52 M), and  $FeCl_2 \cdot 4H_2O$  (0.26 M) were mixed and heated (80 °C) under continuous stirring (120 rpm), and pH was adjusted to 10 by adding NaOH 1 M dropwise, then it was stirred for 1 h. The black precipitate was collected and washed several times with distilled water and finally with ethanol, and dried at 70 °C for 24 h. The magnetic FeO particles were added to chitosan gel (1:2 mass ratio), mixed for 1 h, and sonicated for 30 min at room temperature. The beads of chitosan-FeO were formed as described above, and to prepare DES modified chitosan-FeO beads (Ch-FeO-DES) after washing, excess water was removed with filter paper, and beads were mixed with freshly prepared DES (proportion 1/1, w/w), vacuum was applied overnight at 60 °C, and finally they were washed and dried at room temperature.

# 2.3. Characterization

Infrared spectra were obtained by Attenuated Total Reflection (ATR) Spectroscopy using a Nicolet 6700 equipment (Thermo Scientific) connected to a diamond crystal ATR accessory (Smart Orbit). Sample spectra were recorded at an angle of incidence of  $45^{\circ}$  (one reflection) in the range from 400 to  $4000 \, \mathrm{cm}^{-1}$  with a resolution of  $4 \, \mathrm{cm}^{-1}$  and using a DTGS detector. A total of 34 scans were performed for each sample.

Scanning electron microscopy (SEM) was applied to obtain the surface morphology of the beads. The samples were deposited on the stubs using conductive self-adhesive carbon tabs and then coated with a thin layer of gold using an Emitech K550 sputter coater. Structural characterization was performed using a JEOL JSM 6700F field emission SEM microscope.

Brunauer-Emmett-Teller (BET) surface area analysis and Barrett-Joyner-Halenda (BJH) pore size and volume analysis were performed using the system TriStar II Plus 3030 (Micromeritics, Inc.) and data were processed using the software Version 3.00 (Micromeritics). The samples were degassed for 3 h at 25 °C and 0.11 mbar using the SmartVacPrep 067 (Micromeritics, Inc.). The isotherms were obtained using nitrogen gas (99.999% purity, Alphagaz-1, purchased to Air Liquide, Spain) at 77.41 K (immersed in liquid nitrogen).

Point of zero charge of the adsorbents was determined using the salt addition technique [24]: a pre-defined amount of adsorbent was added to a series of solutions of NaNO<sub>3</sub> 0.1 M at different pHs (adjusted with 0.1 M NaOH or 0.1 M HCl), in the range 3–11, the samples were shaken for 16 h and final pH were registered. The point of zero charges were obtained from the plot of  $\Delta$ pH against initial pH.

### 2.4. Adsorption experiments

Dye solutions were prepared by weight, in the range 25–250 mg/L. The solutions were used without modification of pH. The experiment series testing the pH effect required previous pH adjustment, and the solutions were adjusted to pH 3.5, 6, 8 and 10 with NaOH 0.1 M or HCl 0.1 M, alternatively.

Batch adsorption experiments were carried out, varying the different conditions: adsorbent dosage (0.005–0.035 g), initial dye concentration (25–250 mg/L), contact time (15–480 min), pH (3–10) and temperature (25–45 °C), with continuous shaking at 350 rpm

in a Ohaus orbital shaker model ISHD16HDG. Four adsorption experiment series were carried out at various conditions of adsorbent dosage, initial dye concentration, pH and temperature, as indicated in Table 1. The pH of all the solutions was measured at the beginning of the experiment and at the end, with a pH-meter Hanna, model HI5221. The volume of the solutions was maintained at 5 mL in all the experiments. The variation in the dye concentration was determined by absorbance data obtained at a wavelength of 626 nm, using a UV-VIS spectrometer Jasco V-750.

A preliminary screening of the three adsorbents with AB80 dye was carried out at the following conditions: ratio adsorbent mass/ dye solution volume was fixed at 5 g/L, the initial dye concentration was  $100 \, \text{mg/L}$ , the temperature was  $25 \, ^{\circ}\text{C}$  and the contact time, 6 h. The best adsorbent was selected for further study of adsorption equilibrium and kinetics. A summary of experimental conditions is shown in Table 1.

The concentration of the dye uptake by the adsorbents at equilibrium  $(q_e, mg/g)$ , and at time t  $(q_t)$ , and the removal percentage of the dyes were determined by the equations 1–3:

$$q_e = \frac{V(C_0 - C_e)}{m}$$

$$q_t = \frac{V(C_0 - C_t)}{m}$$

Dye removal 
$$\% = \frac{C_0 - C_t}{C_0} \times 100$$

where  $C_0$ ,  $C_t$ , and  $C_e$ , are the concentrations of dye at the start, at time t, and at equilibrium, respectively. V is the dye volume in L and m is the adsorbent mass in g. The presented results were the mean of replicate experiments, at least 2, until a variation coefficient lower than 10% was obtained.

# 2.5. Adsorption kinetics

Different adsorption kinetics models were used for analyzing the results obtained: pseudo-first and pseudo-second order models (Eqs. S2 and S3, respectively), Elovich kinetic model (Eq. S4) and intraparticle diffusion (Eq. S5) [14,25–29].

# 2.6. Adsorption isotherm

Diverse isotherm models, including Langmuir, Freundlich, Temkin and Dubinin–Radushkevich have been evaluated [8]. These models, as well as Elovich isotherm model, were used in present work, to study the affinity, trend, and adsorption mechanism of analyte towards sorbent. Equations 4–11 represent the mentioned models, respectively [30–34]:

$$\frac{C_e}{q_e} = \frac{1}{q_m K_L} + \frac{C_e}{q_m} \tag{4}$$

$$log q_e = log k_F + \frac{1}{n} log C_e$$
 5

$$q_e = B \ln K_T T + B \ln C_e$$

where:  $C_e$  is concentration of adsorbate at equilibrium (final concentration of solute (mg/L)/liquid-phase concentrations of dye at equilibrium);  $q_e$  is the amount of dye adsorbed at equilibrium (mg/g);  $K_L$  (L/mg or L/mol) is Langmuir constant related to adsorption capacity (mg g<sup>-1</sup>), which can be correlated with the variation of the suitable area and porosity of the adsorbent, implying that large surface area and pore volume will result in higher adsorption capacity. It is calculated from the intercept of the different straight lines (linear plot of  $C_e/q_e$  vs.  $C_e$ ) at different temperatures.  $K_F$  denotes Freundlich constant, and is adsorption capacity (L/mg) and 1/n is adsorption intensity; it also indicates the relative distribution of the energy and the heterogeneity of the adsorbate sites.  $K_T$  is Temkin isotherm constant (L g<sup>-1</sup>). T (°K) is the absolute temperature. R represents the universal gas constant (8.314 J mol<sup>-1</sup>K<sup>-1</sup>). B = RT/b is a constant which is related to the heat of adsorption (J mol<sup>-1</sup>);  $q_m$  is the maximum amount of dye adsorbed (mg/g)/maximum monolayer adsorption capacity (calculated from the slope of the different straight lines at different temperatures).

The value of the dimensionless constant called the separation factor, based on the following equation (7) could be used to predict

 Table 1

 Summary of the conditions of experimental tests.

Series	Dye concentration (mg/L)	Adsorbent	Adsorbent weight (g)	Temperature (°C)	pH value
0	100	un-Ch, Ch-DES, Ch-FeO-DES	0.025	25	7
1	100	Ch-DES	0.005, 0.010, 0.015, 0.025, 0.035	25	7
2	25, 50, 100, 150, 200, 250	Ch-DES	0.015	25	7
3	25, 50, 100, 150, 200, 250	Ch-DES	0.015	25, 35, 45	7
4	100	Ch-DES	0.015	25	3.5, 6, 7, 8, 10

the degree of favourability of the Langmuir isotherm for equilibrium data [30]:

$$R_L = \frac{1}{1 + K_L C_{max}}$$

where  $K_L$  is Langmuir constant and  $C_{max}$  is the maximum initial concentration of adsorbate.  $R_L$  values indicate the adsorption to be unfavourable when  $R_L > 1$ , linear when  $R_L = 1$ , favorable when  $0 < R_L < 1$ , and irreversible when  $R_L = 0$  [35].

Dubinin-Radushkevich isotherm is expressed as follows (Eq. 8):

$$\ln q_r = \ln q_m - \beta \varepsilon^2$$

$$\varepsilon = RT \ln \left( 1 + \frac{1}{C_e} \right)$$

$$E = \frac{1}{\sqrt{2\beta}}$$

where  $\varepsilon$  is Polanyi potential,  $\beta$  is Dubinin-Radushkevich constant, R is gas constant (8.31 Jmol<sup>-1</sup> K<sup>-1</sup>), T is absolute temperature, and E is mean adsorption energy [35].

The Elovich isotherm linear form is expressed as follows (Eq. 11):

$$\ln\frac{q_e}{C_e} = \ln k_e q_m - \frac{q_e}{C_e}$$

Elovich maximum adsorption capacity and Elovich constant can be calculated from the slope and intercept of the plot of  $ln(q_e/C_e)$  vs  $q_e$  [35].

### 2.7. Thermodynamic study

The adsorption of AB80 was studied at different temperatures: 25, 35 and 45  $^{\circ}$ C, at original dye pH 7, 0.015 g of adsorbent, and 5 mL of dye solutions at all the concentrations tested, 25, 50, 100, 150, 200 and 250 mg/L. Gibbs free energy change,  $\Delta G$  (kJ/mol), enthalpy change,  $\Delta H$  (kJ/mol), and the change in entropy,  $\Delta S$  (kJ/mol K), were calculated to obtain information about the adsorption process. The equations used were (Eq. 12–13):

$$\Delta G = -RT \ln k_c$$

Where:  $k_c = \frac{q_e}{C}$ 

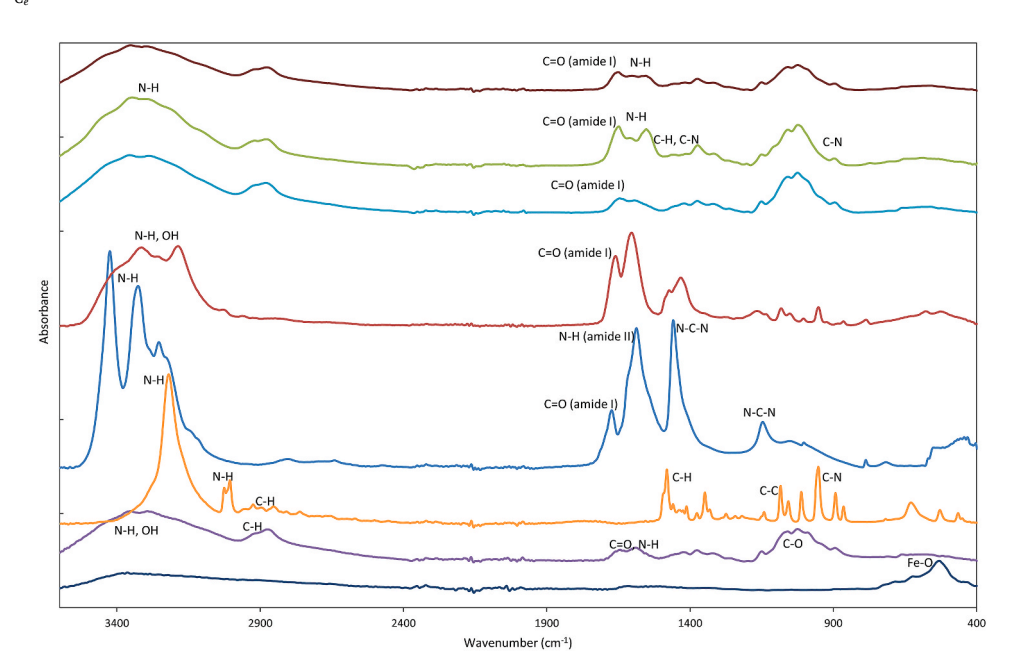


Fig. 1. Fourier transform infrared (FTIR) spectra of the starting materials FeO (—), chitosan (——), choline chloride (—ChCl), urea (—), Deep eutectic solvent choline chloride:urea (—DES ChCl:U) 1:2, and the chitosan-based adsorbents used in this work: unmodified chitosan (—un-Ch) beads, DES-modified chitosan (—Ch-DES) beads, and DES modified chitosan-FeO (—Ch-FeO-DES) beads.

 $\Delta H$  and  $\Delta S$  were calculated using Van't Hoff equation (Eq. 13):

$$\ln k_c = \frac{\Delta S}{R} - \frac{\Delta H}{R_T}$$

### 2.8. Reusability tests

Desorption experiments and reusability tests were also done, using NaOH 0.1 M and  $H_2SO_4$  0.1 M, and applying the same experimental conditions as for adsorption tests. Three desorption cycles were performed, then, the adsorbent was tested for reuse.

Additionally, the reusability of untreated adsorbent was examined 5 times using  $0.015\,\mathrm{g}$  of adsorbent,  $5\,\mathrm{mL}$ ,  $100\,\mathrm{mg/L}$  initial AB80 concentration for  $360\,\mathrm{min}$  contact time at  $25\,\mathrm{^{\circ}C}$ .

### 3. Results and discussion

### 3.1. Adsorbent characterizations

# 3.1.1. Fourier transform infrared (FTIR) spectrum

Fig. 1 shows the FTIR spectra of the adsorbents and individual components used to elaborate them. Chitosan (as raw material) and chitosan beads (un-Ch beads) exhibit broad bands at 3352 and 3294 cm<sup>-1</sup>, corresponding to the stretching vibration of N-H and -OH functional groups. At 2875-2920 cm<sup>-1</sup>, the bands correspond to stretching vibration of C-H bonds in CH, CH<sub>2</sub> and CH<sub>3</sub> groups. The bands around 1025 and 1059 cm<sup>-1</sup> are attributed to C-O-C and C-OH stretching vibrations, respectively, associated with the carboxyl and hydroxyl groups in the chitosan structure The characteristic bands observed at 1645 and 1592 cm<sup>-1</sup>, indicating stretching vibration of C=O and bending of N-H in amide groups, are representative of primary amine of highly deacetylated chitosan for amide I (CONH<sub>2</sub>) and II (N-H), respectively. The appearance of amide I groups has been mainly attributed to the cross-linking process in the formation of ionic interactions and hydrogen bonding with the acetic acid [23].

Regarding Choline chloride, characteristic bands observed are: the corresponding to stretching vitrations of N–H bonds at 3219,  $3006-3026~\rm cm^{-1}$ ; the bands at  $1413-1481~\rm cm^{-1}$ , that may be assigned to alkyl groups (bending of aliphatic C–H groups), or N–H vibrations in quaternary ammonium groups (bands within the range of  $1480-1390~\rm cm^{-1}$ ) [36]; bands within the range  $1200-880~\rm cm^{-1}$ , especially the band at  $953~\rm cm^{-1}$ , corresponding to asymmetric C–N stretching vibration, and bands  $2854-2951~\rm cm^{-1}$ , assigned to alkyl groups (stretching vibrations of C–H bond in CH<sub>2</sub> and CH<sub>3</sub>).

Urea shows the main bands at 3425-3326 cm<sup>-1</sup>, assigned to asymmetric N-H stretching vibration of NH<sub>2</sub> groups, at 3228-3254 cm<sup>-1</sup>, assigned to symmetric N-H stretching vibration of NH<sub>2</sub> groups, at 1674 cm<sup>-1</sup>, assigned to stretching vibration of C=O in amide group (CONH<sub>2</sub>) (amide I band), 1587 cm<sup>-1</sup>, assigned to bending of N-H bond in NH<sub>2</sub> groups (amide II band), and finally, 1459 and 1147, assigned to asymmetric and symmetric stretching vibration of N-C-N bonds, respectively [37].

Concerning Deep eutectic solvent ChCl:Urea (1:2), a broadening of the bands in the 3500-3000 cm<sup>-1</sup> region is observed, probably

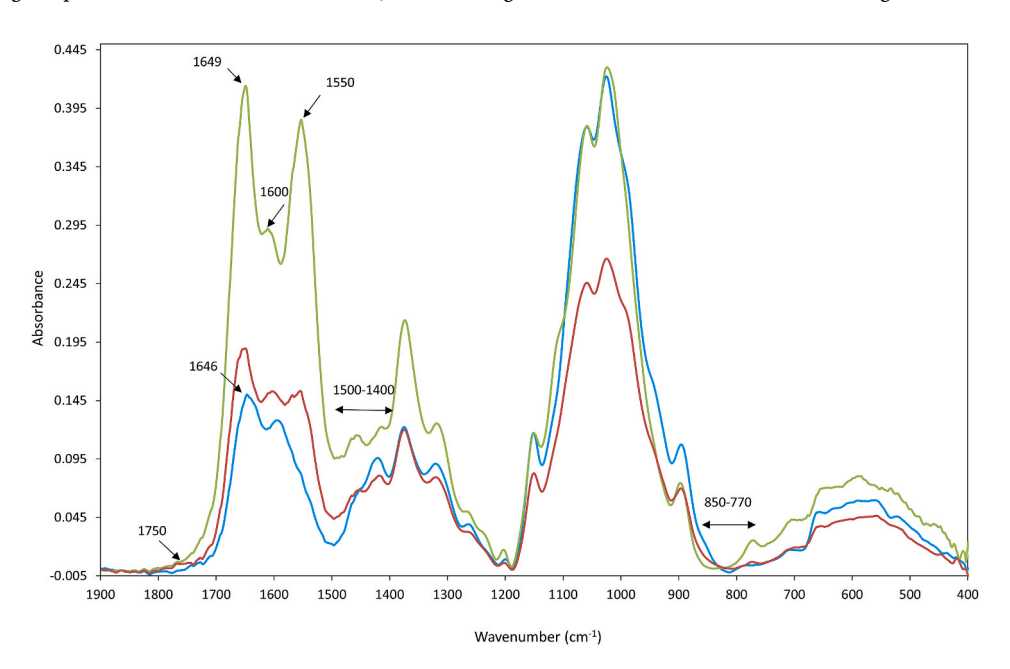


Fig. 2. Fourier transform infrared (FTIR) spectra focused on the spectral differences among the chitosan-based adsorbents used in this work: unmodified chitosan (—un-Ch) beads, DES-modified chitosan (—Ch-DES) beads, and DES modified chitosan-FeO (—Ch-FeO-DES) beads.

caused by the formation of hydrogen bonds between hydrogen bond acceptor (HBA) and hydrogen bond donnor (HBD). Then, bands at 3388 and 3314 cm<sup>-1</sup> can be assigned to stretching vibration of N–H and O–H bonds, and at 3256 and 3187 cm<sup>-1</sup> can be assigned to stretching vibration of N–H. In addition, C=O stretching vibration band of amide group CONH has shifted to lower frequencies (1660 cm<sup>-1</sup>), compared to urea (at 1674 cm<sup>-1</sup>). Similar findings have been reported by Jakubowska et al. (2020) for DES ChCl:malonic acid (1:1) [36]. Then, the interaction between the components in DES causing the decrease in melting point of the mixture ChCl:Urea can be confirmed by the changes in FTIR spectra.

Results from FTIR analysis show spectral differences between DES-modified chitosan beads and unmodified chitosan beads (Fig. 2), indicating possible attachment of the functional groups. Chitosan showed two bands in the region 1500-1700 cm<sup>-1</sup>, where the stretching vibration of C=O and bending of N-H bonds of amide occur (present in urea and also in chitosan). In this region, 3 bands can be clearly observed now in DES-modified chitosan beads: a band at 1550 cm<sup>-1</sup> arises with high intensity, and this new band, together with the 1600 cm<sup>-1</sup> band, are more intense as DES concentrations increase in DES-modified beads (data not shown). This new band at 1550 cm<sup>-1</sup>, and the band at 1600 cm<sup>-1</sup>, could be also assigned to bending of N-H bonds of amide and NH<sub>2</sub> groups. In addition, the band at 1646 cm<sup>-1</sup> in the chitosan beads (stretching vibration of C=O of amide I group) slightly shifts to 1649 cm<sup>-1</sup> in chitosan-DES beads, and a significant increase in the area under this peak can be observed in Ch-DES beads compared to Ch beads, indicating that this band is being contributed by other C=O band corresponding to urea from the DES. This change confirms the attaching of DES molecules to chitosan beads, since the intensity of the bands would reflect a rise of N-H and C=O groups coming from the urea in DES.

A new peak at around 1750 cm<sup>-1</sup> can be observed, although it is a small band, and may correspond to C=O stretching vibration (in carboxylic groups characteristic of HBD: urea). This band was also observed in mixtures of chitosan with DES ChCl:malonic acid (1:1) [36]. Other regions that might show a change in the intensity or shape of the spectral bands are: the region 1400-1500 cm<sup>-1</sup> (bending of aliphatic C-H bonds and asymmetric stretching vibration of C-N bond in urea) and, to a lower extent, in the region 850-770 cm<sup>-1</sup> (symmetric stretching vibration of C-N bonds, in ChCl). There's also a change in the band around 3200 cm<sup>-1</sup>, more defined in DES-modified adsorbents, and assigned to stretching vibration of N-H.

The spectra of DES modified chitosan-FeO (Ch-FeO-DES) beads reflects changes in the same bands as described above for Ch-DES beads, however, these changes occur at a lower intensity. The typical bands described for magnetite,  $Fe_3O_4$ , at  $531\,\mathrm{cm}^{-1}$ , corresponding to stretching vibration of Fe–O are observed in our FeO particles, however, it is not detected in the Ch-FeO-DES beads, and only a very slight increase in the intensity was registered in the adsorbent. Then, FeO particles incorporated in the Ch-FeO-DES beads were negligible in the adsorbent surface.

### 3.1.2. Scanning electron microscopy (SEM)

Fig. 3 shows the morphology of the adsorbents un-Ch, Ch-DES and Ch-FeO-DES obtained by scanning electron microscopy (SEM). The beads are spherical-ovoid in all cases (Fig. S2), the average diameter size was 965.7, 948.5 and 1088.6  $\mu$ m, respectively. Un-Ch shows a smooth area with some minor cavities on the surface. By contrast, Ch-DES shows areas with smooth surface, and areas with rougher surface exhibiting more cavities and small pores. Ch-FeO-DES shows protuberances distributed along the beads smooth surface, and the FeO nanoparticles are visible only on those particular spots.

# 3.1.3. Brunauer-Emmett-Teller (BET) and Barrett-Joyner-Halenda (BJH) analysis

The surface area, volume and pore size of the beads were determined by the Brunauer-Emmett-Teller (BET) and Barrett-Joyner-Halenda (BJH) analysis. Results are shown in Table 2.

The porosity was very low in the three adsorbents. The small pore volume and pore size of the beads used in our work were similar to the chitosan beads prepared by others [23] or slightly higher [20], as well as the size of the beads. Slightly higher values of pore volume and pore size were observed in Ch-FeO-DES beads, probably owing to the presence of FeO nanoparticles; however, their distribution on the beads'surface seems to be restricted to scarce single spots, as commented above (Fig. 3).

# 3.2. Preliminary screening and selection of the best adsorbent/dye

Fig. 4 shows the AB80 adsorption data obtained after testing the three different adsorbents at an initial AB80 concentration of 100 mg/L and ratio adsorbent mass/dye solution volume of 5 g/L.

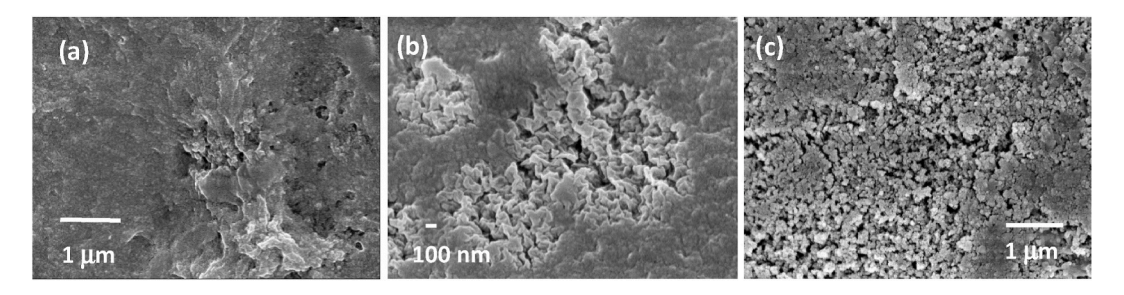


Fig. 3. Scanning electron microscopy (SEM) images of the adsorbents unmodified chitosan (a) un-Ch, (b) chitosan-DES (Ch-DES) and (c) chitosan modified with FeO and DES (Ch-FeO-DES) beads.

Table 2
Brunauer-Emmett-Teller (BET) and Barrett-Joyner-Halenda (BJH) analysis related to the surface area and porosity of the adsorbents unmodified chitosan (un-Ch), chitosan-DES (Ch-DES) and chitosan modified with FeO and DES (Ch-FeO-DES) beads.

	un-Ch	Ch-DES	Ch-FeO-DES
BET surface area (m <sup>2</sup> /g)	0.34	0.15	0.27
pore volume (cm <sup>3</sup> /g)	$3.6 \times 10^{-4}$	$1.5 \times 10^{-4}$	$4.3\times10^{-4}$
pore size (nm)	4.16	4.05	6.54
micropore surface area (m <sup>2</sup> /g)	0.54	0.23	0.42

The Ch-DES beads adsorb the dye AB80 at a relatively high rate, in comparison with the remaining tested beads: a sharp increase in the adsorption during the first 30 min of the experiment is exhibited, in contrast to the smoother adsorbance increase shown by un-Ch and Ch-FeO-DES. Afterwards, Ch-DES adsorption continues to increase more moderately until the adsorption capacity achieves 19.6 mg/g at 120 min, with 95.9% removal from water. From this moment, after a slight increase in removal up to the maximum values, 99.3% removal from water, the Ch-DES adsorption process reaches the equilibrium state. The sharp increase in the removal rate and adsorption capacities during the initial stage of the experiment could be due to the fast diffusion on the surface and formation of a film onto the Ch-DES beads, with a higher number of binding sites (functional groups attached during DES modification of chitosan beads) than the other assayed adsorbents.

Un-Ch and Ch-FeO-DES show a similar adsorption rate, with a faster adsorption by Ch-FeO-DES beads, reaching the maximum capacity and the equilibrium state at  $300 \, \text{min}$ , with a removal rate of 91.5% and adsorption of  $18.2 \, \text{mg/g}$ , and later, at  $360 \, \text{min}$ , in the adsorbent un-Ch, with similar removal and adsorption values, 89.7% and  $17.7 \, \text{mg/g}$ , respectively.

The Ch-DES beads adsorption capacity at equilibrium reaches a maximum value (19.6 mg/g) higher than Ch-DES-FeO and un-Ch (18.2 and 17.7 mg/g, respectively) and faster: at 120 min, compared to 300 and 360 min, respectively, when used with the dye AB80. Then, the more efficient AB80 adsorbent, Ch-DES, was selected for further study of adsorption equilibrium and kinetics.

### 3.3. Factors affecting the adsorption process

### 3.3.1. Adsorbent dose

The adsorbent dosage effect on the removal percentage and adsorption of AB80 in aqueous solution was tested to obtain the optimal dosage providing the best performance at the lowest adsorbent spent. Fig. 5 shows the results obtained. At increasing doses of adsorbent Ch-DES beads, more removal rate is obtained, while the adsorption capacity per unit weight (adsorbent) decreases. The surface area of adsorbent increases when higher adsorbent quantity is used, so the availability of active binding sites on the adsorbent allows a higher removal efficiency.

The most efficient dose to our objectives was 0.015 g of adsorbent per 5 mL of AB80 solution of an initial concentration of 100 mg/L, since the removal achieves the maximum value and the equilibrium state. At higher adsorbent doses, there was no further increase in the dye removal. This finding can be attributed to a screening effect at increasing adsorbent doses due to accumulation of adsorbent particles and the decrease in the distance between them. Binding sites for AB80 molecules might be hidden by coacervates on the adsorbent surface; furthermore, adsorbent overlap leads to competition among AB80 molecules for a limited number of available binding sites, and increased diffusion path length, resulting in a decrease in the adsorption rate [38–40].

# 3.3.2. Initial dye concentration and contact time

The effect of contact time and initial concentrations of AB80 on the removal efficiency of Ch-DES beads are shown in Fig. 6. It can be seen that during the first step of the adsorption process, the adsorption was very fast, and then it continued to increase more gradually during a second step, to finally achieve an equilibrium state where no more adsorption takes place. The duration of each stage and the

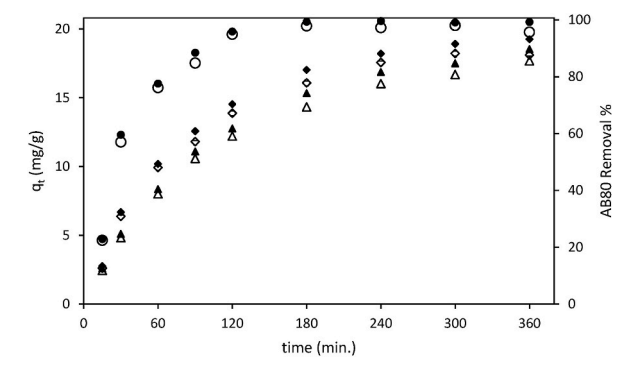


Fig. 4. Effect of the different adsorbents and contact time on the amount of dye adsorbed  $(q_t)$ :  $(\Delta)$  un-Ch,  $(\circ)$  Ch-DES,  $(\diamondsuit)$  Ch-FeO-DES; and the dye removal from the aqueous solution (AB80 removal %) at 25 °C by a ratio adsorbent mass/dye solution volume of 5 g/L:  $(\blacktriangle)$  un-Ch,  $(\clubsuit)$  Ch-DES,  $(\clubsuit)$  Ch-FeO-DES

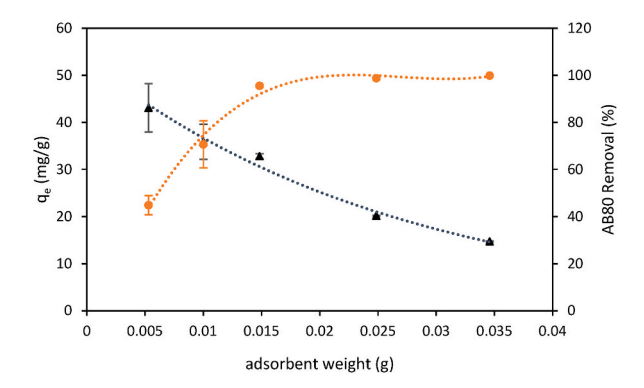


Fig. 5. Effect of the different adsorbent Ch-DES dosage on the removal efficiency ( ) and the amount of dye adsorbed (qe) ( ) for 5 h at 25 °C from 5 mL of 100 mg/L AB80 solution.

dye elimination rate is dependent on the initial AB80 concentration of the solutions: at the lowest AB80 concentration, 25 mg/L, the elimination rate is very sharp during the first 60 min, and it continues to increase at a lower rate the next 30 min, until equilibrium is reached, within the first 90 min. At increasing concentrations, the rate of dye elimination is especially sharp the first 60 min, and the subsequent increase in the removal is more moderate, the higher the dye initial concentration, the lower the dye removal rate (Fig. 6). Consistently, the equilibrium state is reached at different times, and the dye removal achieves different efficiencies, depending on the initial concentration: the more AB80 initial concentration, the more duration of the process until the equilibrium is achieved, and the lower the removal efficiency. The AB80 removal percentage reached 98–100% at initial concentrations of 25–100 mg/L, within 5 h. More time was needed at higher initial concentrations, about 8 h to reach 93% (150 mg/L), 80% (200 mg/L) and up to 10–15h to reach 71% (250 mg/L). The rapid removal rate at the beginning of the process could be explained by the high availability of active adsorption sites on the beads surface. The surface diffusion of the dye molecules onto the adsorbent through the solution that occurs at the first stage is influenced by the concentration of the dye solution, and the agitation and time [41]. The lower removal at higher initial dye concentrations may be explained by the mass transfer resistance between the adsorbate and adsorbent caused by the increase in the concentration gradient. The sites become occupied by the dye molecules and cause an increase in the time of contact between adsorbate and adsorbent, and repulsion forces increase between the adsorbed dye and the dye molecules in the liquid phase [42].

The adsorption capacity increased very fast at the beginning of the process, the higher the initial AB80 concentration, the faster the increase and the higher the adsorption value achieved (Fig. S3). This may be explained by the concentration gradient increase with the increasing dye concentration, that would compensate the mass transfer resistance between the adsorbate and adsorbent [42]. The adsorption capacity values found were 8.25, 16.80, 33.95, 46.39, 52.91 and 58.39 mg/g for AB80 concentrations of 25, 50, 100, 150, 200 and 250 mg/L, respectively, at 25 °C, and pH 7.

# 3.3.3. Temperature

The influence of the temperature on the removal of AB80 by Ch-DES beads was tested: the adsorption experiments were carried out at 25, 35 and 45  $^{\circ}$ C. A slight increase in dye removal, up to 2%, can be observed when the temperature rises from 25 to 35  $^{\circ}$ C, probably due to an increase in the diffusion rate. By contrast, a decrease was registered when the temperature rises from 35 to 45  $^{\circ}$ C, when the initial dye concentrations were 150, 200 and 250 mg/L (Fig. S4). A removal decrease of around 10% was observed at 45  $^{\circ}$ C in the mentioned solutions. The decrease in dye removal at increasing temperatures indicates that the adsorption process is exothermic. These observations could be explained by the desorption of the adsorbed AB80 molecules caused by the destruction of adsorption

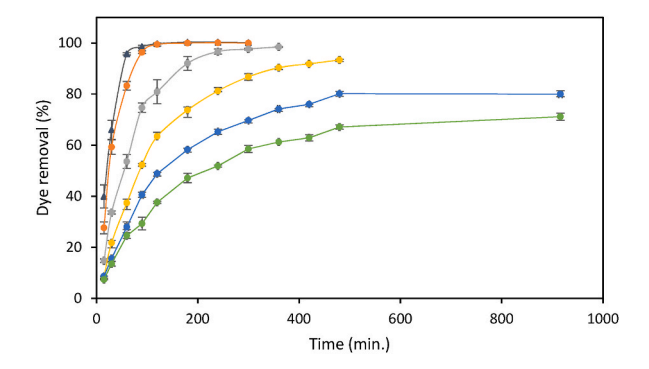


Fig. 6. Effect of Acid Blue 80 dye concentrations and contact time on the removal (%) of the dye adsorbed at 25 °C and pH 7 by 15 mg of Ch-DES beads: (a) 25 mg/L, (e) 100 mg/L, (e) 150 mg/L, (e) 200 mg/L, (e) 250 mg/L. (For interpretation of the references to colour in this figure legend, the reader is referred to the Web version of this article.)

forces that were responsable for the elimination of adsorption interactions between active sites of the beads and the dye molecules [42]. As a consequence, the best temperature for adsorption in this case is 25 °C.

# 3.3.4. pH

The binding of dye molecules onto adsorbents is affected by the pH, since the degree of dissociation and/or ionization of dye molecules and the adsorbent surface is influenced by this parameter. The functional groups occurring in the adsorbent, such as amine and hydroxyl groups, are affected by the pH of the dye solution, as reported [43].

Fig. S5 shows the influence of the initial pH value on the removal of AB80 by Ch-DES beads. The pH effect was tested at a pH range of 3.5–10, the initial concentration of AB80 was 100 mg/L, and the dye removal was tested at 219 min. The removal percentage was higher at lower pH: at pH 3.5, 100% of AB80 was removed, while at the highest pH tested, pH 10, the removal was the lowest, 83%. At intermediate pH values, lower than 7, the removal was higher than 95%.

The adsorption of AB80 onto the Ch-DES beads was affected by pH, with a decrease above pH 7. This observation agrees with the obtained point of zero charge (pHpzc), 6.98, for Ch-DES beads (Fig. S6): at pH lower than pHpzc, the adsorbent is positively charged, then, at acidic conditions, amine groups of adsorbent were protonated, and the negative sulfonate ions of AB80 were probably adsorbed by electrostatic attraction, explaining the highest removal efficiency at pH 3.5 [43]. The decrease in removal with increasing pH from 3.5 to 7 might be due to the reduction in the amount of protonated amino groups on the adsorbent, leading to a decreasing electrostatic attraction between the dye molecules and the Ch-DES beads. At pHs higher than 6.98, Ch-DES beads are negatively charged, so the adsorption capacity decreases at a higher rate owing to repulsions between the anionic dye and the adsorbent surface.

It has been reported that the pH of the dyeing discharge from textile industry generally ranges from 9 to 11 [44]; although lower, the Ch-DES beads efficiency was significant at pH 10 (83% AB80 removal).

### 3.4. Adsorption kinetic models

Adsorption kinetics brings information to understand the adsorption process: the potential controlling steps and the adsorption mechanism. The literature provides a lot of studies applying different adsorption kinetic models for removal of dyes molecules using chitosan-based adsorbents, such as first-order-kinetic, pseudo-second-order-kinetic, intraparticle diffusion and Elovich [8].

The adsorption of AB80 on Ch-DES beads was studied under different initial concentrations to investigate the most appropriate adsorption kinetics model. The pseudo-second-order (Fig. 7), pseudo-first order, Elovich and intraparticle diffusion (Weber-Morris model) (Figs. S7–S9) kinetics linear graphs were represented; linear plots of  $\ln (q_e-q_t)$  vs t,  $t/q_t$  vs t,  $q_t$  vs  $\ln(t)$ , and  $q_t$  vs  $t^{1/2}$ , respectively, were used to obtain the values. Table 3 shows the adsorption kinetic parameters  $k_1$ ,  $k_2$ ,  $k_3$ ,  $q_e$ , I,  $\beta$  and  $\alpha$ , corresponding to the different models, calculated using the linear plots, together with the parameter  $R^2$ .

The linear fit and regression coefficient values obtained for the studied kinetic models point at the pseudo-second order (Fig. 7) as the more suitable model throughout all the AB80 concentrations. There is also good agreement between the values of calculated  $q_e$  (pseudo second-order) and the experimental  $q_e$  exp, although the model obtains higher  $q_e$  values, about 25% on average, when the concentration of AB80 was higher than  $100 \, \text{mg/L}$  (Table 3). At these higher AB80 concentrations, a better agreement between the calculated  $q_e$  by the pseudo-first-order model and the experimental  $q_e$  were obtained (Fig. S7).

The value of the pseudo-second-order rate constant,  $k_2$ , was inversely proportional to the dye concentration tested, as reported in different studies [42].

The rate of adsorption of AB80 onto Ch-DES beads is a function of the number of sites available for adsorption and also the concentration of dye molecules in the solution, as the pseudo-second-order model assumes; surface adsorption is the dominating process [8]. The rate-limiting step would be determined by the chemical adsorption, depending on the electrostatic forces through the electrons exchange [23].

Description of the adsorption mechanism using the intraparticle diffusion model: The adsorption of AB80 at low concentrations

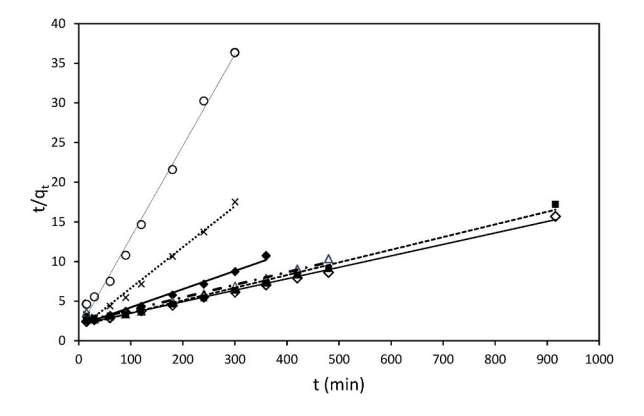


Fig. 7. Pseudo-second order sorption kinetics of AB80 at 25 °C by 15 mg of Ch-DES beads, at different AB80 initial concentrations: ( $\circ$ ) 25 mg/L, (x) 50 mg/L, (x) 100 mg/L, (x) 100 mg/L, (x) 100 mg/L, (x) 200 mg/L, (x) 250 mg/L.

**Table 3**Parameters of the kinetic models for AB80 adsorption on Ch-DES beads.

Dye	AB80						
concentration (mg/L)	25	50	100	150	200	250	
q <sub>e</sub> , exp (mg/g)	8.25	16.80	33.95	46.39	52.91	58.39	
Pseudo-first order kinetic	model						
k <sub>1</sub> (1/min)	$66.8\times10^{-3}$	$49.5\times10^{-3}$	$17.2\times10^{-3}$	$10.9 \mathrm{x} \ 10^{-3}$	$9.0\times10^{-3}$	$5.9\times10^{-3}$	
q <sub>e</sub> (mg/g)	16.29	33.47	42.42	55.56	63.43	56.40	
$R^2$	0.9771	0.9715	0.9700	0.9444	0.9314	0.9917	
Pseudo-second order kine	etic model						
k <sub>2</sub> (mg/(g min))	$9.1 \times 10^{-3}$	$1.8\times10^{-3}$	$0.3\times10^{-3}$	$0.1\times10^{-3}$	$0.1\times10^{-3}$	$0.1\times10^{-3}$	
q <sub>e</sub> (mg/g)	8.65	19.35	43.51	62.96	62.57	69.15	
$\mathbb{R}^2$	0.9935	0.9896	0.9812	0.9755	0.9913	0.9961	
Elovich kinetic model							
β (g/mg)	0.639	0.241	0.103	0.076	0.073	0.0687	
$\alpha  (mg/(g  min))$	1.771	1.399	1.154	1.105	1.194	1.174	
$R^2$	0.7478	0.8799	0.9791	0.9920	0.9699	0.9782	
Intraparticle diffusion kir	netic model						
$k_3  (mg/(g  min^{1/2}))$	0.295	0.819	1.897	2.341	2.012	2.196	
I	4.116	5.523	2.748	1.038	6.452	4.983	
R <sup>2</sup>	0.5567	0.7156	0.8879	0.9325	0.8438	0.8898	

(25–100 mg/L) would take place in two steps (Figs. S10a–c): the first indicates the formation of a film onto the adsorbent, with fast diffusion on the surface. The second, a decrease in the particle adsorption, since most of the dye molecules were already adsorbed. By contrast, at higher AB80 concentrations (150–250 mg/L), the process can be divided in three stages (Figs. S10d–f): the first, with the fast diffusion on the surface and formation of a film onto the adsorbent; the second, with a slow particle diffusion between the AB80 films that were formed during the first stage; and the third stage, with a decrease in the adsorption rate owing to the absence of available active sites.

At higher concentrations, especially at 250 mg/L, the pseudo-first model would partially explain the experimental data: during the initial stage, the kinetics is governed by the rate of surface reactions, and when the system approaches equilibrium, there is a change in the predominant mechanism from surface reactions to intraparticle diffusion [45].

### 3.5. Adsorption isotherms

The isotherm of dyes adsorption was studied at three different temperatures: 25, 35 and 45 °C (Fig. 8). The adsorption data was used to construct the linear plots of  $C_e/q_e$  vs  $C_e$ , log  $(q_e)$  vs  $\log(C_e)$ ,  $q_e$  vs  $\ln(C_e)$ ,  $\ln(q_e)$  vs  $\varepsilon^2$  and  $\ln(q_e/C_e)$  vs  $q_e$ , and the correlation coefficient,  $R^2$ , was used to fit the data to the Langmuir (Fig. 9), Freundlich, Temkin, Dubinin-Radushkevich and Elovich isotherm models (Figs. S11a–d). The values of  $K_L$ ,  $K_F$ ,  $K_T$ ,  $\beta$ ,  $K_e$ ,  $q_m$ , n, B, were calculated from the linear plots and are shown on Table S2.

From the obtained results, we can conclude that the experimental data of AB80 adsorption onto Ch-DES beads fitted with Langmuir isotherm model with  $R^2 > 0.99$  at all the temperatures tested, suggesting the adsorption process takes place by the formation of a monolayer of colourant molecules on uniform distribution of sorption sites in the adsorbent, without interactions among adsorbed molecules [23]. When the process reaches the equilibrium state, the saturation of the monolayer would be complete [20].

The separation factor constant,  $R_L$ , estimating the degree of suitability of adsorbent to dye, increased at increasing temperatures, but the obtained values, around 0.01 (Table S2), indicated that the adsorption process is very favorable (0 <  $R_L$  < 1) [35], in our conditions.

Our results also fit well with Temkin isotherm at the lowest temperature tested,  $25 \,^{\circ}\text{C} \, (\text{R}^2 > 0.99)$  and also at 35 and  $45 \,^{\circ}\text{C} \, (\text{R}^2 > 0.97)$ . The parameter B, related to the heat of adsorption, decreases with increasing temperature, from 7.36 (25  $^{\circ}\text{C}$ ) to

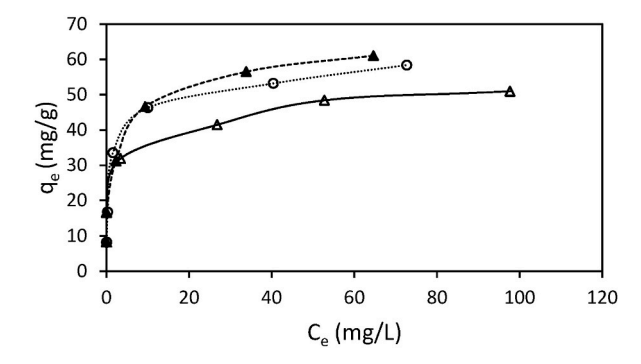


Fig. 8. The isotherms of AB80 adsorption on Ch-DES beads at different temperatures: (ο) 25, (Δ) 35 and (Δ) 45 °C.

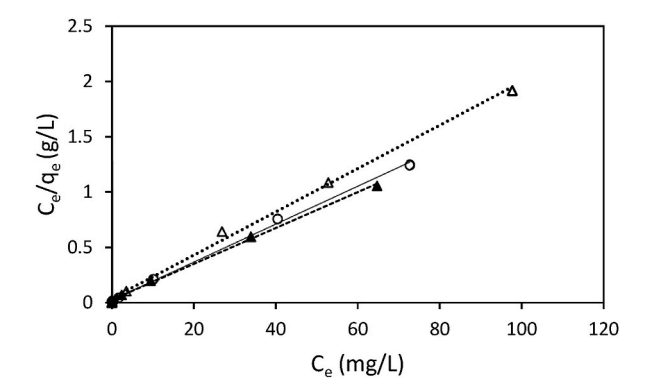


Fig. 9. Langmuir isotherm for the adsorption of AB80 by 15 mg of Ch-DES beads at (o) 25, (A) 35 and ( $\Delta$ ) 45 °C, and pH 7.

4.82 J/mol ( $45 \,^{\circ}\text{C}$ ). The Temkin isotherm constant,  $K_T$ , increases with increasing temperature, from a value of  $0.14 \,(25 \,^{\circ}\text{C})$  to  $0.99 \,\text{L/g}$  ( $45 \,^{\circ}\text{C}$ ) (Table S2). The Temkin adsorption model describes the interaction between the adsorbate, adsorbent and indirect effects in adsorption isotherms; Temkin equation introduces the influence of temperature on the adsorption based on Langmuir model. Therefore, we can conclude that AB80 adsorbs onto Ch-DES beads uniformly on a monolayer, and the heat of adsorption of molecules in the layer decreases linearly as a result of increase surface coverage [35].

The mean energy of adsorption may be deduced from the Dubinin-Radushkevich isotherm: the low positive value of E (0.3–0.5 kJ/mol) indicates a low potential barrier, suggesting a physical nature of the adsorption process [46].

# 3.6. Thermodynamic study

Thermodynamic parameters were calculated from the linear plots of  $ln(k_c)$  and 1/T ( $k_c = q_e/c_e$ ) (Fig. S12), and are summarized on Table S3. Negative values obtained for the parameter  $\Delta G$  at all temperatures and dye concentrations, except the highest (250 mg/L of AB80), and the concentration 200 mg/L when temperature was 45 °C, indicate that the adsorption process is spontaneous except at the previously mentioned conditions. At increasing AB80 concentrations, and at increasing temperatures, the  $\Delta G$  values shift to more positive values, meaning that the adsorption process becomes less favorable. A similar trend was described for the adsorption of metanil yellow dye on a chitosan-based adsorbent [47]. By contrast, at the lowest AB80 concentrations tested, 25 and 50 mg/L, the  $\Delta G$  values shift to more negative values at increasing temperatures (Table S3). The  $\Delta H$  values, negative when the concentrations of dye were above 100 mg/L, confirm the exothermic nature of the adsorption process at those conditions. Then, we can conclude that at lower concentration of the AB80 molecules in the solution, the process is endothermic, so the increase in temperature helps adsorption. On the contrary, at higher concentration of AB80 molecules, the process is exothermic, so the adsorption is favoured at lower temperatures.

The values of  $\Delta G$  obtained are in the range (-20) to 0 kJ/mol generally described for physisorption [46]. The negative values of the enthalpy change, in the range (-13.9) to (-42.6) kJ/mol, would indicate that the adsorption involves weak forces of attraction, of physical nature, and the process, exothermic at values of dye concentration above 100 mg/L, is energetically stable [46]. The negative

# Reusability test - untreated beads

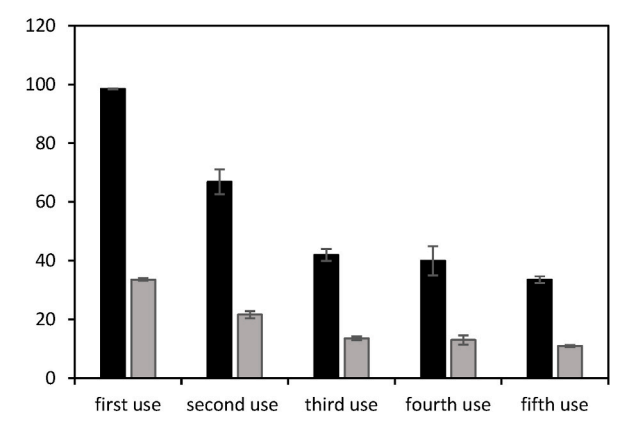


**Fig. 10.** Results of reusability of not desorbed Ch-DES beads, during 5 successive adsorption tests, at 100 mg/L initial AB80 concentration, 15 mg of adsorbent, 25 °C, 350 rpm, and 6 h contact time: (■) dye removal %, (■) adsorption (mg/g).

 $\Delta S$  values at the mentioned range of dye concentrations reflected the decreased randomness at the solid-liquid interface during the adsorption of dye onto adsorbent.

# 3.7. Reusability of the adsorbent

The results obtained during reuse of untreated (not desorbed) Ch-DES beads after each adsorption process is shown on Fig. 10 The adsorbent partially maintains the adsorption capacity, and continues eliminating the dye AB80 from the aqueous solution, at a lower rate after the first use, 66.8%, and with a further decrease, around 40%, ater the next uses. It is even capable of removing 33.6% of AB80 from the solution after 5 uses.

### 3.7.1. Desorption

The results of desorption experiments, using NaOH 0.1 M and  $H_2SO_4$  0.1 M, and applying the same experimental conditions as for adsorption tests, are shown on Fig. 11. Three desorption cycles were performed, and as it can be seen, the desorption percentage was very high when NaOH was used, in the range 80–99%, but it was notably lower, from 30 to 6%, when  $H_2SO_4$  was used. Two cycles of treatment with NaOH were very effective to desorb the dye AB80 from the Ch-DES beads. It was also shown that at increasing initial dye concentration used during the adsorption, the percentage of desorption with NaOH also increased, however, the opposite was observed when  $H_2SO_4$  was used. During NaOH treatment, a competition between the OH $^-$  ions and the anionic dye molecules adsorbed to Ch-DES beads might be responsable for the elution of AB80, as described by others [47,48].

Afterwards, the adsorbents treated by both methods were tested for reuse. Fig. 12 shows the obtained results when NaOH 0.1 M was used to desorb the beads. There was a decrease in the removal of AB80 from the solution, from 98% to 43%. Therefore, the desorption process with NaOH was not practical for application when the material was intended for reuse, but it could be a very effective way to recover the dye.

Concerning the adsorbent treated with  $H_2SO_4$  0.1 M, the results obtained when it was reused for AB80 adsorption are shown on Fig. 13. Although AB80 desorption was negligible, the Ch-DES beads were still capable of eliminating ca. 100% of the dye AB80 from a 100 mg/L solution, even after 5 successive uses. In addition, the adsorption capacity after each use remains at the same value. This result suggests that the Ch-DES beads have increased their adsorption capacity after the acid treatment, probably due to protonation of the amine groups of chitosan, and therefore, improving the electrostatic interaction with the anionic dyes and facilitating their removal, as reported by others [49].

### 3.8. Possible adsorption mechanism

The FTIR spectra of Ch-DES beads after AB80 adsorption, shows the Ch-DES beads typical bands together with the characteristic bands of the dye AB80 (Fig. S13). Some differences are observed in the beads after adsorption, compared to the beads before use, in the stretching vibration of C–H groups (between 2848 and 2963 cm<sup>-1</sup>) as well as the stretching vibration of O–H and N–H groups (around 3300 cm<sup>-1</sup>), indicating that the dye AB80 was incorporated to the Ch-DES beads. Additionally, several peaks not present in the adsorbent before use, are observed in the Ch-DES-AB80-adsorbed, and come from the dye: in the region from 400 to 2000 cm<sup>-1</sup>, the bands at 1594, 1576, 1491, 1451, 1364, 1075, 994, 841, 820, 801, 726, 673, 625, 579, 555, 512, and 470 cm<sup>-1</sup>. No obvious new peak was detected, and peaks in the region 1790-1284 cm<sup>-1</sup> decreased after adsorption, this would mean that the interaction adsorbent-pollutant is mainly of physical nature [48].

The adsorption and desorption behavior of AB80 on the studied adsorbent, Ch-DES beads, was possibly affected by the electrostatic interactions: when the OH<sup>-</sup> ions were present, they would replace the anionic dye molecules adsorbed to Ch-DES beads and eluted them from the adsorbent, and conversely, when protonation of the amine groups of chitosan takes place by addition of acid, enhancement of the electrostatic interaction with the anionic dye molecules would improve their adsorption to the Ch-DES surface.

Overall, the adsorption behavior at lower AB80 concentrations appeared to be dominated by chemisorption, depending on the electrostatic attraction, onto Ch-DES beads surface, with a rapid diffusion from the solution to the adsorbent favoured by increasing temperature. However, at higher AB80 concentrations, the process seemed also ruled by physisorption, with an initial rapid diffusion from the solution to the adsorbent followed by a slow particle diffusion caused by mass transfer resistance, and increased repulsion forces between the dye molecules in the adsorbent and the liquid phase, and finally a saturation of available active sites. Besides, at the higher AB80 concentration range, the process was exothermic and hence the increase in temperature induced a decreased adsorption. In addition, the free energy change became less favorable at increasing AB80 concentrations.

### 3.9. Comparison of Ch-DES adsorption capacities with other adsorbents

The adsorption capacity values (Qm) in the literature, showed differences among different adsorbent materials. Lower values compared with our adsorbent were obtained for AB80 when a  $CuTiO_2$  composite was used (22.23 mg/g) [16]. Other adsorbents were reported to reach higher capacities, such as activated carbon from vegetal residues, with values in the range 88.03–294.7 mg/g [50, 51], chemical modified bentonites, with 126–201 mg/g [52,52,53], and Al-based metal organic framework (MOF), with 200 mg/g [53].

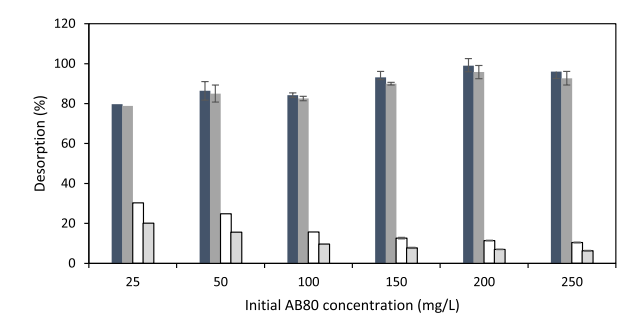
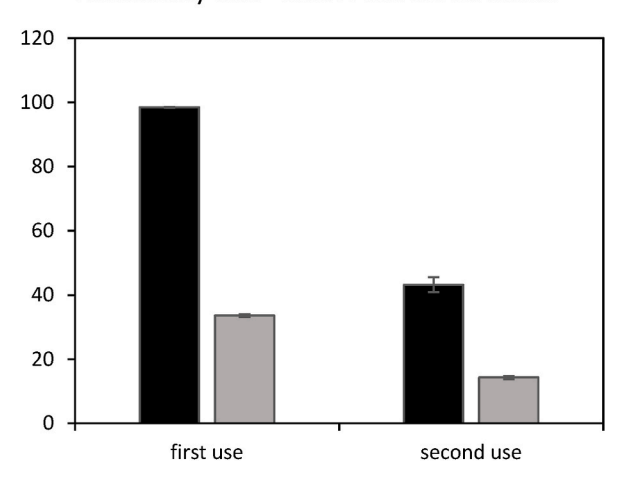


Fig. 11. Results of desorption of AB80 from Ch-DES beads applying NaOH 0.1 M or  $H_2SO_4$  0.1 M during 3 successive desorption cycles (25 °C, 350 rpm): ( $\blacksquare$ ) NaOH, 3 desorption cycles sum; ( $\blacksquare$ ) NaOH, 1st and 2nd desorption cycles sum; ( $\square$ )  $H_2SO_4$ , 3 desorption cycles sum; ( $\square$ )  $H_2SO_4$ , 1st and 2nd desorption cycles sum.

# Reusability test - NaOH-desorbed beads



**Fig. 12.** Results of reusability of NaOH-desorbed Ch-DES beads, at 100 mg/L initial AB80 concentration, 15 mg of adsorbent, 25 °C, 350 rpm, and 6 h contact time: (■) dye removal %, (□) adsorption (mg/g).

# Reusability test - H<sub>2</sub>SO<sub>4</sub> partially-desorbed beads

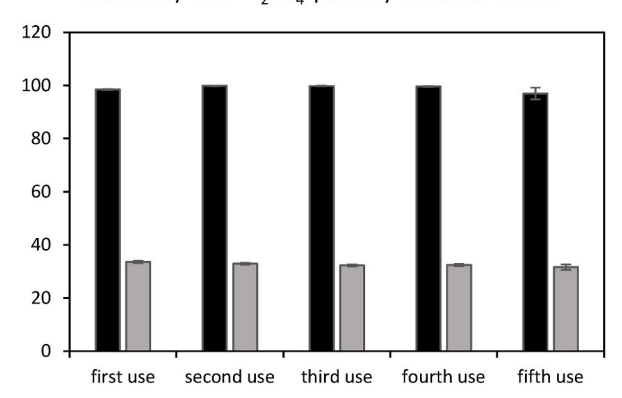


**Fig. 13.** Results of reusability of partially H<sub>2</sub>SO<sub>4</sub>-desorbed Ch-DES beads, during 5 successive adsorption tests, at 100 mg/L initial AB80 concentration, 15 mg of adsorbent, 25 °C, 350 rpm, and 6 h contact time: (■) dye removal %, (■) adsorption (mg/g).

### 4. Conclusions

This work envisages an opportunity to obtain alternative adsorbents based on chitosan modification with deep eutectic solvents (DESs) that offered enhanced adsorption capacity compared to the starting materials. The sorbents could be easily recovered and

reused, and eventual recovery of the dye by desorption was possible. Successful modification of chitosan beads using a deep eutectic solvent of choline chloride:urea allowed to improve substantially the capacity of chitosan itself to adsorb the dye Acid Blue 80. Below dye concentrations of 100 mg/L, the removal percentages were as high as 98–100%, and for 250 mg/L -the highest concentration tested- they were still around 71%. The adsorption process could be described with the pseudo-second-order kinetic model and the monolayer Langmuir isotherm. Sorbent recovery and reuse was feasible, with an extremely high efficiency (100% dye removal) during several cycles after acid treatment of the beads. The adsorption process required mild operating conditions: at temperature lower than 35 °C, the adsorption was optimum and spontaneous, and worked for a wide pH range, which makes it applicable to typical effluents discharged from the textile industry. It can also be extended to other anionic dyes (e.g. azo type), and its industrial application could contribute to the development of alternative green and sustainable technologies for water remediation and circular economy.

# Declaration of competing interest

The authors declare that they have no known competing financial interests or personal relationships that could have appeared to influence the work reported in this paper.

# Data availability

Data will be made available on request.

### Acknowledgement

This work was supported by Agencia Estatal de Investigación (Spain) (PID2019-107728RB-IOO/AEI/10.13039/501100011033 and Xunta de Galicia (GPC-ED431B 2020/08).

Authors would like to thank Estefanía López and Marcin Grzelczak, for their valuable contributions on Fourier Transform Infrared Spectroscopy and Scanning Electron Microscopy, respectively, performed at CACTI facilities of Universidade de Vigo, and Alberto Núñez, on Brunauer-Emmett-Teller (BET) and Barrett-Joyner-Halenda (BJH) analyses performed at SAI facilities of Universidade da Coruña.

# Appendix A. Supplementary data

Supplementary data to this article can be found online at https://doi.org/10.1016/j.wri.2022.100195.

### References

- [1] D.C. da Silva Alves, B. Healy, L.A. de A. Pinto, T.R.S. Cadaval, C.B. Breslin, Recent developments in Chitosan-based adsorbents for the removal of pollutants from aqueous environments, Molecules 26 (2021), https://doi.org/10.3390/molecules26030594.
- [2] European Environment Agency, n.d. https://www.eea.europa.eu/publications/textiles-in-europes-circular-economy. (Accessed 20 July 2022) https://www.eea.europa.eu/publications/textiles-in-europes-circular-economy.
- [3] A. Sutlović, M.I. Glogar, I. Čorak, A. Tarbuk, Trichromatic vat dveing of cationized cotton, Materials 14 (2021), https://doi.org/10.3390/ma14195731.
- [4] W.J. Epolito, Y.H. Lee, L.A. Bottomley, S.G. Pavlostathis, Characterization of the textile anthraquinone dye Reactive Blue 4, Dyes Pigments 67 (2005) 35–46, https://doi.org/10.1016/j.dyepig.2004.10.006.
- [5] European Chemicals Agency (Echa) (n.d.), https://echa.europa.eu/substance-information/-/substanceinfo/100.022.500.
- [6] Environment Canada Health Canada, Screening assessment for the challenge benzenesulfonic acid, 3,3'-[(9,10-dihydro-9,10-dioxo-1,4-anthracenediyl) diimino]bis[2,4,6-trimethyl-, disodium salt (Acid Blue 80). https://www.ec.gc.ca/ese-ees/69053600-E5FE-4200-A263-69A7B9E8CC9D/batch2\_4474-24-2\_en. pdf, 2008. (Accessed 20 July 2022).
- [7] S. Arslan, M. Eyvaz, E. Gürbulak, E. Yüksel, A review of state-of-the-art technologies in dye-containing wastewater treatment the textile industry case, Textil. Wastewater Treat.Intech (2016), https://doi.org/10.5772/64140.
- [8] N. Aramesh, A.R. Bagheri, M. Bilal, Chitosan-based hybrid materials for adsorptive removal of dyes and underlying interaction mechanisms, Int. J. Biol. Macromol. 183 (2021) 399–422, https://doi.org/10.1016/j.ijbiomac.2021.04.158.
- [9] M.T. Yagub, T.K. Sen, S. Afroze, H.M. Ang, Dye and its removal from aqueous solution by adsorption: a review, Adv. Colloid Interface Sci. 209 (2014) 172–184, https://doi.org/10.1016/j.cis.2014.04.002.
- [10] N.K. Soliman, A.F. Moustafa, Industrial solid waste for heavy metals adsorption features and challenges; a review, J. Mater. Res. Technol. 9 (2020) 10235–10253, https://doi.org/10.1016/j.jmrt.2020.07.045.
- [11] O.S. Bello, O.A. Olusegun, V.O. Njoku, Fly ash: an alternative to powdered activated carbon for the removal of eosin dye from aqueous solutions, Bull. Chem. Soc. Ethiop. 27 (2013) 191–204, https://doi.org/10.4314/bcse.v27i2.4.
- [12] M.S.U. Rehman, I. Kim, J.I. Han, Adsorption of methylene blue dye from aqueous solution by sugar extracted spent rice biomass, Carbohydr. Polym. 90 (2012) 1314–1322, https://doi.org/10.1016/j.carbpol.2012.06.078.
- [13] A. Demirbas, Agricultural based activated carbons for the removal of dyes from aqueous solutions: a review, J. Hazard Mater. 167 (2009) 1–9, https://doi.org/10.1016/j.jhazmat.2008.12.114.
- [14] N.K. Soliman, A.F. Moustafa, H.R.A. El-Mageed, O.F. Abdel-Gawad, E.T. Elkady, S.A. Ahmed, H.S. Mohamed, Experimentally and theoretically approaches for disperse red 60 dye adsorption on novel quaternary nanocomposites, Sci. Rep. 11 (2021), https://doi.org/10.1038/s41598-021-89351-9.
- [15] N.K. Soliman, A.F. Moustafa, A.A. Aboud, K.S.A. Halim, Effective utilization of Moringa seeds waste as a new green environmental adsorbent for removal of industrial toxic dyes, J. Mater. Res. Technol. 8 (2019) 1798–1808, https://doi.org/10.1016/j.jmrt.2018.12.010.
- [16] I.J. Puentes-Cárdenas, G.M. Chávez-Camarillo, C.M. Flores-Ortiz, M.D.C. Cristiani-Urbina, A.R. Netzahuatl-Muñoz, J.C. Salcedo-Reyes, A.M. Pedroza-Rodríguez, E. Cristiani-Urbina, Adsorptive removal of acid blue 80 dye from aqueous solutions by Cu-TiO2, J. Nanomater. (2016), https://doi.org/10.1155/2016/3542359, 2016.

- [17] A.M. el Nahrawy, A.M. Bakr, Nano-architecture of CaO/Ag-chitosan nanocomposite by sol gel process: formation and characterization, Egypt, J. Chem. 64 (2021) 7393–7406, https://doi.org/10.21608/EJCHEM.2021.80608.3995.
- [18] L. Villar Blanco, O. González Sas, P.B. Sánchez, Á. Domínguez Santiago, B. González de Prado, Congo red recovery from water using green extraction solvents, Water Resour. Ind. 27 (2022), https://doi.org/10.1016/j.wri.2021.100170.
- [19] Y. Dai, K.H. Row, Magnetic chitosan functionalized with β-cyclodextrin as ultrasound-assisted extraction adsorbents for the removal of methyl orange in wastewater coupled with high-performance liquid chromatography, J. Separ. Sci. 41 (2018) 3397–3403, https://doi.org/10.1002/jssc.201800177.
- [20] A.C. Sadiq, N.Y. Rahim, F.B.M. Suah, Adsorption and desorption of malachite green by using chitosan-deep eutectic solvents beads, Int. J. Biol. Macromol. 164 (2020) 3965–3973, https://doi.org/10.1016/j.ijbiomac.2020.09.029.
- [21] I.A. Lawal, T.H. Dolla, K. Pruessner, P. Ndungu, Synthesis and characterization of deep eutectic solvent functionalized CNT/ZnCo 2 O 4 nanostructure: kinetics, isotherm and regenerative studies on Eosin y adsorption, J. Environ. Chem. Eng. 7 (2019), https://doi.org/10.1016/j.jece.2018.102877.
- [22] G. Li, K.H. Row, Deep eutectic solvents skeleton typed molecularly imprinted chitosan microsphere coated magnetic graphene oxide for solid-phase microextraction of chlorophenols from environmental water, J. Separ. Sci. 43 (2020) 1063–1070, https://doi.org/10.1002/jssc.201901159.
- [23] D.A. Patiño-Ruiz, G. de Ávila, C. Alarcón-Suesca, Á.D. González-Delgado, A. Herrera, Ionic cross-linking fabrication of chitosan-based beads modified with FeO and TiO2nanoparticles: adsorption mechanism toward naphthalene removal in seawater from cartagena bay area, ACS Omega 5 (2020) 26463–26475, https://doi.org/10.1021/acsomega.0c02984.
- [24] L.S. Silva, L.C.B. Lima, F.J.L. Ferreira, M.S. Silva, J.A. Osajima, R.D.S. Bezerra, E.C. Silva Filho, Sorption of the anionic reactive red RB dye in cellulose: assessment of kinetic, thermodynamic, and equilibrium data, Open Chem. 13 (2015) 801–812, https://doi.org/10.1515/chem-2015-0079.
- [25] D. Rady, M. Shaban, K.N.M. Elsayed, A. Hamd, N.K. Soliman, H.R. Abd El-Mageed, A.M. Elzanaty, R. El-Sayed, M. Morada, S.M. El-Bahy, S.A. Ahmed, Experimentally and theoretically approaches for Congo red dye adsorption on novel kaolinite-alga nano-composite, Int. J. Environ. Anal. Chem. (2021), https://doi.org/10.1080/03067319.2021.1969378.
- [26] A. Hamd, M. Shaban, H. Almohamadi, A.R. Dryaz, S.A. Ahmed, K.A. Abu Al-Ola, H.R. Abd El-Mageed, N.K. Soliman, Novel wastewater treatment by using newly prepared green seaweed-zeolite nanocomposite, ACS Omega 7 (2022) 11044–11056, https://doi.org/10.1021/acsomega.1c06998.
- [27] F.C. Wu, R.L. Tseng, R.S. Juang, Initial behavior of intraparticle diffusion model used in the description of adsorption kinetics, Chem. Eng. J. 153 (2009) 1–8, https://doi.org/10.1016/j.cei.2009.04.042.
- [28] W.J. Weber, C.J. Morris, Advances in Water Pollution Research: Removal of Biologically Resistant Pollutant from Wastewater by Adsorption., in: 1st International Conference on Water Pollution Symposium, Pergamon Press, Oxford, 1962, pp. 231–266, 2.
- [29] W.J. Weber, J.C. Morris, Kinetics of adsorption on carbon from solutions, J. Sanit. Eng. Div. Am. Soc. Civ. Eng. 89 (1963) 31–60, https://doi.org/10.1061/ JSEDAL.0000430.
- [30] I. Langmuir, The adsorption of gases on plane surfaces of glass, mica and platinum, J. Am. Chem. Soc. 40 (1918) 1361–1403, https://doi.org/10.1021/ia02242a004
- [31] H. Freundlich, Over the adsorption in solution, J. Phys. Chem. A 57 (1906) 1100-1107, https://doi.org/10.1515/zpch-1907-5723.
- [32] M.I. Temkin, V. Pyzhev, Kinetic of ammonia synthesis on promoted iron catalysts, J. Phys. Chem. USSR. 13 (1939) 851–857.
- [33] M.M. Dubinin, L.V. Radushkevich, Equation of the characteristic curve of activated charcoal, Proc. Acad. Sci. USSR Phys. Chem Sect. 55 (1947) 331-333.
- [34] S.Y. Elovich, O.G. Larinov, Theory of adsorption from solutions of non electrolytes on solid (I) equation adsorption from solutions and the analysis of its simplest form, (II) verification of the equation of adsorption isotherm from solutions, Izv. Akad. Nauk. SSSR, Otd. Khim. Nauk. 2 (1962) 209–216.
- [35] N. Ayawei, A.N. Ebelegi, D. Wankasi, Modelling and interpretation of adsorption isotherms, J. Chem. (2017), https://doi.org/10.1155/2017/3039817, 2017.
- [36] E. Jakubowska, M. Gierszewska, J. Nowaczyk, E. Olewnik-Kruszkowska, Physicochemical and storage properties of chitosan-based films plasticized with deep eutectic solvent, Food Hydrocolloids 108 (2020), https://doi.org/10.1016/j.foodhyd.2020.106007.
- [37] M. Manivannan, S. Rajendran, Investigation of inhibitive action of urea-Zn2+ system in the corrosion control of carbon steel in sea water, J. Eng. Sci. Technol. 3 (2011) 8048–8060. https://www.researchgate.net/publication/267782937.
- [38] A. Hamd, D. Rady, M. Shaban, K.N.M. Elsayed, H. al Mohamadi, A.M. Elsanaty, S.A. Ahmed, R. El-Sayed, N.K. Soliman, Application of nano bio-clay composite in a scaling-up study for wastewater treatment, Biointerface Res. Appl. Chem. 12 (2022) 6393–6414, https://doi.org/10.33263/BRIAC125.63936414.
- [39] A.R. Dryaz, M. Shaban, H. AlMohamadi, K.A.A. Al-Ola, A. Hamd, N.K. Soliman, S.A. Ahmed, Design, characterization, and adsorption properties of Padina gymnospora/zeolite nanocomposite for Congo red dye removal from wastewater, Sci. Rep. 11 (2021), https://doi.org/10.1038/s41598-021-00025-y.
- [40] H.S. Mohamed, H.R. Abd El-Mageed, H.S. Ali, T.R. Mahmoud, S.A. Ahmed, N.K. Soliman, Adsorption of Mn+7 ions on chitosan/cellulose composite: experimentally and theoretically approaches, J. Dispersion Sci. Technol. 43 (2021) 1525–1542, https://doi.org/10.1080/01932691.2021.1877555.
- [41] A.C. Sadiq, A. Olasupo, W.S.W. Ngah, N.Y. Rahim, F.B.M. Suah, A decade development in the application of chitosan-based materials for dye adsorption: a short review, Int. J. Biol. Macromol. 191 (2021) 1151–1163, https://doi.org/10.1016/j.ijbiomac.2021.09.179.
- [42] N.K. Soliman, A.F. Moustafa, H.R.A. El-Mageed, O.F. Abdel-Gawad, E.T. Elkady, S.A. Ahmed, H.S. Mohamed, Experimentally and theoretically approaches for disperse red 60 dye adsorption on poyel quaternary nanocomposites. Sci. Rep. 11 (2021), https://doi.org/10.1038/s41598-021-89351-9.
- [43] F.A. Ngwabebhoh, M. Gazi, A.A. Oladipo, Adsorptive removal of multi-azo dye from aqueous phase using a semi-IPN superabsorbent chitosan-starch hydrogel, Chem. Eng. Res. Des. 112 (2016) 274–288, https://doi.org/10.1016/j.cherd.2016.06.023.
- [44] C. Shen, Y. Shen, Y. Wen, H. Wang, W. Liu, Fast and highly efficient removal of dyes under alkaline conditions using magnetic chitosan-Fe(III) hydrogel, Water Res. 45 (2011) 5200–5210, https://doi.org/10.1016/j.watres.2011.07.018.
- [45] S. Sheshmani, A. Ashori, S. Hasanzadeh, Removal of Acid Orange 7 from aqueous solution using magnetic graphene/chitosan: a promising nano-adsorbent, Int. J. Biol. Macromol. 68 (2014) 218–224, https://doi.org/10.1016/J.IJBIOMAC.2014.04.057.
- [46] A.S. Özcan, B. Erdem, A. Özcan, Adsorption of acid blue 193 from aqueous solutions onto BTMA-bentonite, Colloids Surf. A Physicochem. Eng. Asp. 266 (2005) 73–81, https://doi.org/10.1016/j.colsurfa.2005.06.001.
- [47] K.C. Lai, B.Y.Z. Hiew, L.Y. Lee, S. Gan, S. Thangalazhy-Gopakumar, W.S. Chiu, P.S. Khiew, Ice-templated graphene oxide/chitosan aerogel as an effective adsorbent for sequestration of metanil yellow dye, Bioresour. Technol. 274 (2019) 134–144, https://doi.org/10.1016/j.biortech.2018.11.048.
- [48] M. Wu, W. Chen, Q. Mao, Y. Bai, H. Ma, Facile synthesis of chitosan/gelatin filled with graphene bead adsorbent for orange II removal, Chem. Eng. Res. Des. 144 (2019) 35–46, https://doi.org/10.1016/j.cherd.2019.01.027.
- [49] R. Huang, Q. Liu, J. Huo, B. Yang, Adsorption of methyl orange onto protonated cross-linked chitosan, Arab, J. Chem. 10 (2017) 24–32, https://doi.org/10.1016/j.arabic.2013.05.017.
- [50] O. Üner, Acid Blue 80 Removal from Aqueous Solution by Activated Carbon Obtained from Nerium Oleander Fruits, IJPAS (2021), https://doi.org/10.29132/iipas.908703.
- [51] X. Luo, Z. Zhang, P. Zhou, Y. Liu, G. Ma, Z. Lei, Synergic adsorption of acid blue 80 and heavy metal ions (Cu2+/Ni2+) onto activated carbon and its mechanisms, J. Ind. Eng. Chem. 27 (2015) 164–174, https://doi.org/10.1016/j.jiec.2014.12.031.
- [52] F. Gomri, M. Boutahala, H. Zaghouane-Boudiaf, S.A. Korili, A. Gil, Removal of acid blue 80 from aqueous solutions by adsorption on chemical modified bentonites, Desalination Water Treat. 57 (2016). https://www.tandfonline.com/doi/full/10.1080/19443994.2016.1162208. (Accessed 19 July 2022).
- [53] B.M. Jun, J. Heo, N. Taheri-Qazvini, C.M. Park, Y. Yoon, Adsorption of selected dyes on Ti3C2Tx MXene and Al-based metal-organic framework, Ceram. Int. 46 (2020) 2960–2968, https://doi.org/10.1016/j.ceramint.2019.09.293.